bioRxiv preprint doi: https://doi.org/10.64898/2026.11.09.762803; this version posted November 10, 2026. The copyright holder for this preprint (which was not certified by peer review) is the author/funder, who has granted bioRxiv a license to display the preprint in perpetuity. It is made available under a CC-BY 4.0 International license.

Formation of perinuclear actin structures is driven by mechanosensitivity of actin polymerization

Berin Becic[1] and Stephan Gekle[1,*]

[1] *Biofluid Simulation and Modeling, Theoretische Physik VI, Universität Bayreuth, Germany*

(Dated: October 12, 2026)

bioRxiv preprint doi: https://doi.org/10.64898/2026.11.09.762803; this version posted November 10, 2026. The copyright holder for this preprint (which was not certified by peer review) is the author/funder, who has granted bioRxiv a license to display the preprint in perpetuity. It is made available under a CC-BY 4.0 International license.

Abstract

Actin filaments are one of the most dynamic components of the cytoskeleton. Their fast polymerization, particularly in regions around the nucleus, allows the cell to react quickly and efficiently to external mechanical stimuli by controling nucleus morphology and position, thereby influencing the chromatin organization and gene transcription. While the biochemical mechanisms of actin polymerization are well known, the question why polymerization happens most prominently in the perinuclear region has so far remained elusive. Here, we develop a computational model for actin network formation whose key ingredients are: (i) a fully resolved orientational distribution of the local filaments, (ii) a strain-dependent depolymerization rate and (iii) active stress generation by actomyosin motors. With only these ingredients and without any ad-hoc assumptions on the spatial distribution of signaling molecules, our physics-based model explains the formation of perinuclear actin structures after mechanical stimulation as observed experimentally. In addition, our model also provides some insight into the role actin plays in positioning the nucleus, as it predicts the occurrence of a re-centering force when the cell nucleus is displaced, in quantitative agreement with experimental observations.

I. INTRODUCTION

The mechanics of the nucleus plays a central role for cell survivial and function. Mechanical forces exerted on the nucleus can have a decisive influence on cell fate and behavior, e.g. by influencing gene transcription [1–3], blocking multipotency [4] or inducing nuclear envelope rupture which leads to genome instability [5]. As a consequence, protecting the nucleus from unwanted deformation by external forces is a prerequisite for long-term stability of cell function [6–11]. On the other hand, actively generated intracellular forces enable the cell to control the nucleus position and shape which appears to be a key determinant for cell motility in particular in 3D environments [12].

The two key structures for force transmission to the nucleus that have emerged from experimental work of the last decades are the so-called perinuclear actin ring [11, 13] and the nuclear actin cap [7, 11, 14, 15]. In addition to experimental studies, computational models have been developed [7, 16, 17] to capture the mechanical coupling between the

* stephan.gekle@uni-bayreuth.de

bioRxiv preprint doi: https://doi.org/10.64898/2026.11.09.762803; this version posted November 10, 2026. The copyright holder for this preprint (which was not certified by peer review) is the author/funder, who has granted bioRxiv a license to display the preprint in perpetuity. It is made available under a CC-BY 4.0 International license.

cell exterior, the cytoskeleton and the nucleus. These latter studies focussed mostly on the effects of existing actin structures around the nucleus, but did not attempt to clarify in detail the mechanisms which lead to their formation in the first place. For example, it has been observed that the perinuclear actin ring assembles very quickly ($\sim 20s$) upon sudden mechanical stimulation but it is unclear what drives this fast and highly localized assembly [13, 18].

Here, we present a single computational model which encompasses both the formation and the functioning of the perinuclear actin ring. We apply our model to two different prototypical experimental setups. First, our model describes a biophysical mechanism for the formation of an actin ring around the nucleus after a mechanical stimulation of the cell [13, 18]. Second, we explain the re-centering of a displaced nucleus by the formation of an inhomogeneous actin ring which exerts a force on the nucleus directed towards the center [19].

Our starting point are well-established continuum active gel models which have been very successful in capturing a variety of different aspects of the actin cytoskeleton [20–22]. These typically describe the actin network either as isotropic using a scalar concentration field or account for its directionality by using a nematic orientation parameter which describes the local mean orientation of the actin filaments. A series of different works, starting from the one by Deshpande et al. [23], used a more general approach and included a spatially dependent orientation distribution of actin filaments [24–26]. With this, they were able to observe ring-like structures around the nucleus even though they did not study them further [24, 27]. Here, we develop a generic, microscopic model for the polymerization and active stress generation of actin filaments around the nucleus which allows us to explain the actin dynamics for the two prototypical experimental situations introduced above.

II. METHODS

A. Biophysical model

1. *Continuum hypothesis*

The actin structures which we aim to describe consist of individual actin filaments which are cross-linked by a variety of actin binding proteins. For branched actin networks like the

bioRxiv preprint doi: https://doi.org/10.64898/2026.11.09.762803; this version posted November 10, 2026. The copyright holder for this preprint (which was not certified by peer review) is the author/funder, who has granted bioRxiv a license to display the preprint in perpetuity. It is made available under a CC-BY 4.0 International license.

actin cortex or the lamellipodium the length of an individual actin filament lies between $100-1000nm$ [28–30] whereas in stress-fibers they tend to be longer and reach up to $\approx 2\mu m$ [31]. As we are interested to model the actin network on the length scale of the cell ($\sim 30\mu m$) we use a continuum approach and introduce the following two quantities: The number density of actin filaments per angle is denoted as $\eta(\vec{x},\phi)$ and the number of monomers in one actin filament with the respective orientation is denoted as $b(\vec{x},\phi)$. A crucial feature of this description is that these fields not only depend on the spatial coordinate $\vec{x}$ but also on the angle ϕ describing the orientation of the filaments. Such an approach was first introduced by Deshpande et al.[23] and later modified [24–26]. Here, we implicitly assume that the cell is flat (see next section) which is the case for adherent cells. As a result the actin filaments are all oriented approximately in the horizontal plane (parallel to the substrate) and their orientation in that plane can be described by one single angle ϕ. Thus, the number of actin filaments in the volume $d^2\vec{x}$ around $\vec{x}$ and an orientation between ϕ and $\phi + d\phi$ is $\eta(\vec{x},\phi)\cdot d^2\vec{x}d\phi$. The total number density of actin monomers which have polymerized into the network in this volume is $N_\mathrm{b}(\vec{x}) = \int_0^{2\pi}\eta(\phi)\,b(\phi)\,d\phi$.

The dependency of these fields on the angle ϕ describes the geometry of the resulting actin network. For fully aligned filaments, $\eta(\vec{x},\phi)$ is high only along the fiber direction, i.e. $\eta(\vec{x},\phi) \sim \delta(\phi-\phi_0)$ with ϕ_0 the fiber direction. In contrast, for an isotropic network the angular density is constant, i.e. $\eta(\vec{x},\phi) = \eta(\vec{x}), b(\vec{x},\phi) = b(\vec{x})$. Additionally, our description implicitly assumes that all actin filaments at one position which have the same orientation also have the same length. We imagine that this is enforced by the geometric constraints posed by the cross-linking proteins.

To continue, we further assume that no transport of actin filaments occurs. We therefore only describe the incorporation of cytosolic actin filaments into the network. These actin filaments form by the continuous polymerization of actin monomers in the cytosol. This assumption is motivated by the experimental finding that the formation of the perinuclear actin ring is driven by actin polymerization in the vicinity of the nucleus [13], as well as the immobilization of different cell organelles during the formation of the actin ring [18].

bioRxiv preprint doi: https://doi.org/10.64898/2026.11.09.762803; this version posted November 10, 2026. The copyright holder for this preprint (which was not certified by peer review) is the author/funder, who has granted bioRxiv a license to display the preprint in perpetuity. It is made available under a CC-BY 4.0 International license.

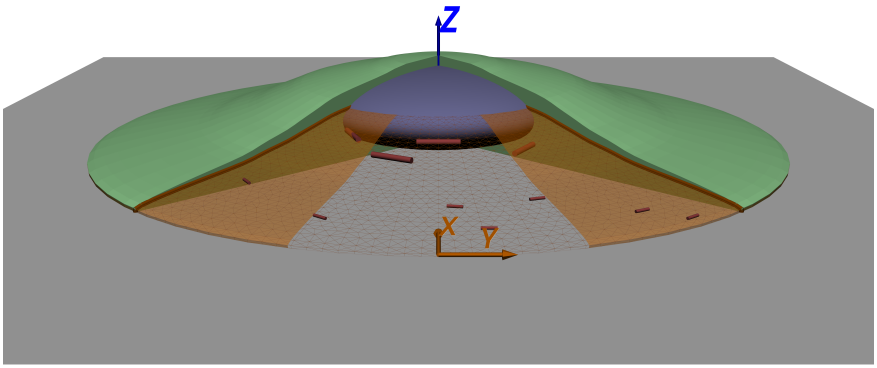


FIG. 1: Illustration of an adhered, relatively flat 3D cell with the cytoskeleton in green and the nucleus in blue. The slice described by our 2D model (orange) starts at the outer edge and follows the cell contour just below the upper surface until it reaches the nucleus.

2. *Cell geometry and passive elasticity*

In agreement with the experimental situations that we attempt to model, we consider a strongly adhering cell whose height is small compared to its lateral extension. Accordingly, we use a two-dimensional description to reduce the computational effort [23, 32, 33]. In three dimensions, the height of the cell is not constant, but decreases towards the edges, described by an elevation profile $h\,(x, y)$. To account for this we consider a two-dimensional slice following the elevation profile of the cell $\frac{z}{h(x,y)} = \text{const}$ rather than a plane at a fixed $z = \text{const}$ as is typically done in 2D formulations. Such a slice is sketched in brown in figure 1. To achieve the best representation, we choose a slice which is relatively close to the upper cell surface but still sufficiently intersects the nucleus. At the edge of the cell, the slice coincides with the substrate to which the cell firmly adheres and one therefore obtains the boundary condition $\vec{u} = 0$ with the displacement $\vec{u}$.

Cytoskeletal components other than actin filaments are considered as a passive elastic continuum and their stresses are modeled using linear elasticity:

$$\sigma_{ij}^{(\text{pass,3D})} = \frac{E\nu}{(1-2\nu)\,(1+\nu)}\epsilon_{kk}\delta_{ij} + \frac{E}{1+\nu}\epsilon_{ij}. \tag{1}$$

Here, E denotes the elastic modulus and ν the Poisson ratio. As usual, ϵ_{ij} represents the

bioRxiv preprint doi: https://doi.org/10.64898/2026.11.09.762803; this version posted November 10, 2026. The copyright holder for this preprint (which was not certified by peer review) is the author/funder, who has granted bioRxiv a license to display the preprint in perpetuity. It is made available under a CC-BY 4.0 International license.

displacement gradient tensor. We apply the free force boundary condition $\sigma_{ij} n_j = 0$ at the upper cell surface.

As the cell is very thin, $\vec{n} \approx \vec{e}_z$ this leads to $0 = \underline{\underline{\sigma}} \cdot \vec{e}_z = (\sigma_{xz}, \sigma_{yz}, \sigma_{zz})$ and thereby implies $\epsilon_{xz} = 0, \epsilon_{yz} = 0, \epsilon_{zz} = -\frac{\nu}{1-\nu}(\epsilon_{xx} + \epsilon_{yy})$. By inserting this back into the three-dimensional stress tensor we obtain the following passive stress tensor:

$$\underline{\underline{\sigma}}^{(\text{pass})} = \begin{pmatrix} \frac{E\nu}{1-\nu^2}(\epsilon_{xx} + \epsilon_{yy}) + \frac{E}{1+\nu}\epsilon_{xx} & \frac{E}{1+\nu}\epsilon_{xy} & 0 \\ \frac{E}{1+\nu}\epsilon_{xy} & \frac{E\nu}{1-\nu^2}(\epsilon_{xx} + \epsilon_{yy}) + \frac{E}{1+\nu}\epsilon_{yy} & 0 \\ 0 & 0 & 0 \end{pmatrix} \tag{2}$$

with all z-components equal zero, such that in the following we only consider the xx, xy, yx and yy component. As reference stress-free state for the passive elasticity, we assume the initial shape.

3. Time evolution of the actin network

To model the time evolution of the actin network we consider two processes: The growth of the network via the incorporation of new actin filaments and the remodeling, i.e. the incorporation of new actin monomers into already bound filaments. Both processes heavily depend on a wide variety of proteins and signaling molecules. As we focus on the mechanosensitive aspects and how they control the nucleus we will for simplicity assume that the biochemical environment is temporarily and spatially constant and favors the polymerization of the actin network. Consequently, the state when an actin filament is bound in the actin network is energetically favorable compared to the unbound state.

a. Incorporation of new actin filaments To start, we consider the growth of the actin network via the incorporation of new actin filaments, as illustrated in figure 2a. Here we assume that once an actin filament with the same number of monomers as those already bound in the network and suitable cross-linkers simultaneously meet at the network they immediately bind to it. This leads to a constant binding rate per unbound filament ω_1 which is limited by the diffusion and the availability of these constituents in the surrounding cytosol. We do not explicitly consider the processes leading to the growth of the actin filaments from the monomeric actin pool in the cytosol, as it is much faster than the incorporation of the filaments into the network. Instead, we estimate the number of suitable actin filaments

bioRxiv preprint doi: https://doi.org/10.64898/2026.11.09.762803; this version posted November 10, 2026. The copyright holder for this preprint (which was not certified by peer review) is the author/funder, who has granted bioRxiv a license to display the preprint in perpetuity. It is made available under a CC-BY 4.0 International license.

which are available for incorporation into the network at any given time to be $\sim \frac{N_\mathrm{u}}{b}$ where N_u denotes the number density of available actin monomers which we assume to be constant throughout the cell as detailed below. This leads to the polymerization rate of the actin network $r_\mathrm{binding} = \omega_1 \frac{N_\mathrm{u}}{b}$.

Next we consider the unbinding process of an actin filament from the network. As this involves the breaking of the cross-linking bonds, the actin filaments have to overcome an energetic barrier $\Delta\mu > 0$ leading to a depolymerization rate per filament $r_\mathrm{unbinding} = \omega_2 e^{-\frac{\Delta\mu}{k_\mathrm{B}T}}$. As the number of cross-links on an individual actin filament increases with the number of monomers it is reasonable to assume that this energy barrier increases linearly with its number of monomers $\Delta\mu = \frac{b}{b_0}\Delta\tilde{\mu}$. Here, b_0 denotes the number of monomers in a fully relaxed actin filament in an undeformed cell. The undeformed state is specified by the reference state of the passive elasticity described in section II A 2. Consequently, $\Delta\tilde{\mu}$ is the binding energy of an actin filament containing b_0 monomers. Then, the time evolution of the concentration of bound actin filaments can be summarized to:

$$\dot{\eta} = \omega_1 \frac{N_\mathrm{u}}{b} - \omega_2 \eta e^{-\frac{b}{b_0}\frac{\Delta\tilde{\mu}}{k_\mathrm{B}T}} \tag{3}$$

Finally, we have to determine the density of unbound actin monomers N_u. We assume that their concentration is spatially constant, as in contrast to the bound actin network the small monomers can diffuse quickly through the cell cytosol. As typical diffusion constants are $D \sim 5\frac{\mu m}{s}$ [34, 35] and the actin ring builds up over $t \sim 40s$, monomers diffuse by $\sqrt{2Dt} \approx 20\mu m$ which corresponds to the typical distance between the periphery and the nucleus in the situations considered here [13, 18]. For the re-centering considered in section III B the time scale of the evolution of the actin structures is even larger. Nevertheless, we did check that allowing a spatially dependent N_u, i.e. neglecting actin monomer diffusion, does not significantly affect our results. The total number density of (bound and unbound) actin monomers can thus be written as

$$N_0 = N_\mathrm{u} + \frac{1}{A_\mathrm{c}} \int_{A_\mathrm{c}} d^2\vec{x} \underbrace{\int_0^{2\pi} d\phi\, \eta(\phi)\, b(\phi)}_{=N_\mathrm{b}} \tag{4}$$

where N_0 depends neither on time nor space, N_u depends on time only and N_b depends on time and space. The cell area excluding the nucleus, where no actin is present, is denoted A_c. Since we consider small deformation only, A_c and coordinates $\vec{x}$ always refer to the undeformed shape.

bioRxiv preprint doi: https://doi.org/10.64898/2026.11.09.762803; this version posted November 10, 2026. The copyright holder for this preprint (which was not certified by peer review) is the author/funder, who has granted bioRxiv a license to display the preprint in perpetuity. It is made available under a CC-BY 4.0 International license.

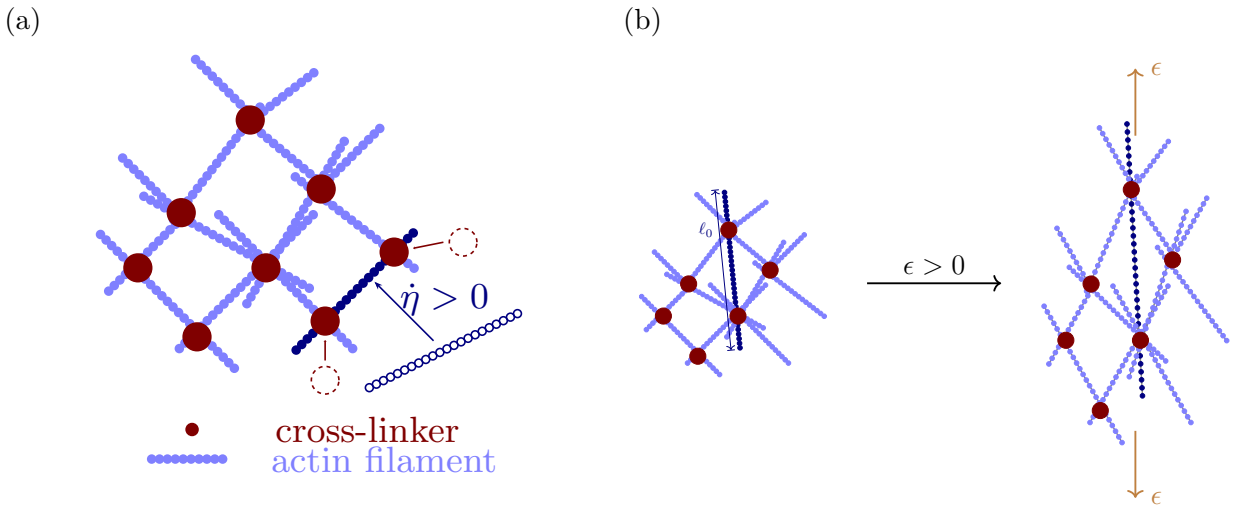


FIG. 2: Illustration of the two basic mechanisms for actin dynamics in our model. (a) sketches the incorporation of new actin filaments in the network (polymerization). (b) illustrates the change of the filament length upon the stretching of the network (remodeling).

b. Remodeling of bound actin filaments Next we describe the remodeling of the actin filaments in the network. To start, we consider an undeformed cell which corresponds to the reference state of the passive elasticity discussed in section II A 2 and an isotropic actin network which is formed in it. We define ℓ_0 as the physical length and b_0 as the number of actin monomers, respectively, in one filament in this state. These quantities will, in general, strongly depend on actin regulating proteins which here are considered to be spatially and temporally constant.

Now, figure 2b illustrates the stretchig of the entire cell from ℓ_0 to $\ell' = \ell_0 (1 + \epsilon)$ which increases the distance between monomers away from the relaxed state distance b_0/ℓ_0. The filament will react by incorporating new monomers until the new equilibrium b_{eq} is reached which fulfills $\frac{\ell'}{b_{\text{eq}}} = \frac{\ell_0}{b_0}$. Inserting ℓ' from above, the new equilibrium is given by $b_{\text{eq}} = b_0 (1 + \epsilon)$ with $\epsilon = \epsilon_{ij} n_i n_j$ being the component of the strain tensor ϵ_{ij} in filament direction. Denoting the filament orientation vector as $\vec{n}$, this strain component is $\epsilon(\phi) = \epsilon_{ij} n_i n_j$. To describe the dynamics of this incorporation, a very simple model is employed, assuming that the

bioRxiv preprint doi: https://doi.org/10.64898/2026.11.09.762803; this version posted November 10, 2026. The copyright holder for this preprint (which was not certified by peer review) is the author/funder, who has granted bioRxiv a license to display the preprint in perpetuity. It is made available under a CC-BY 4.0 International license.

filaments relax exponentially towards their new equilibrium:

$$\dot{b} = -\frac{1}{\tau}\Big[b - \underbrace{b_0\,(1+\epsilon)}_{=b_{\mathrm{eq}}}\Big] \cdot \begin{cases} 1 & \dot{b} < 0 \\ N_{\mathrm{u}}/N_0 & \dot{b} > 0 \end{cases} \tag{5}$$

Here τ is the timescale of the remodeling process and the prefactor N_{u}/N_0 accounts for the effect that the incorporation of new monomers is limited by the availability of actin monomers in the surrounding cytosol.

To sum up, equations (3), (4) and (5) govern the time evolution of the actin filament concentration and their number of monomers for every orientation independently.

c. Steady state To interpret the mechano-sensitivity of the actin network formation resulting from this model, we determine the steady-state concentration of bound actin monomers N_{b} for a uniaxial cell strain ϵ_{yy} which, without loss of generality, is chosen along the y-direction. Note that this leads to an orientation-dependent scalar strain $\epsilon(\phi)$ which is maximal in the y-direction. The concentration of bound actin monomers is obtained from the previously derived time evolution equations of the actin network. Setting $\dot{b} = 0$ in equation (5), we obtain $b = b_{\mathrm{eq}} = b_0\,(1+\epsilon)$ while setting $\dot{\eta} = 0$ in equation (3) yields

$$\eta\,(\phi)\,b\,(\phi) = N_{\mathrm{u}} \underbrace{\frac{\omega_1}{\omega_2} e^{\frac{\Delta\tilde{\mu}}{k_{\mathrm{B}}T}}}_{=\mathrm{const}} e^{\frac{\Delta\tilde{\mu}}{k_{\mathrm{B}}T}\epsilon}. \tag{6}$$

Thus, for small concentrations of bound actin monomers where $N_{\mathrm{u}} \approx N_0 = \mathrm{const}$, the amount of bound actin monomers $\eta \cdot b$ grows exponentially with ϵ_{yy}. For large concentrations, the growth of $\eta \cdot b$ slows down as $N_{\mathrm{u}} \to 0$. This behavior is illustrated in figure 3a where the dependency of the total concentration of bound actin monomers on the uniaxial strain ϵ_{yy} is plotted. For $\epsilon_{yy} = 0$, we obtain the reference concentration in the unstressed state $N_{\mathrm{b}}^{\mathrm{ref}}/N_0 \approx 0.34$.

Next, we consider anisotropic cell strain. Then, the steady-state concentration of filaments in each direction will depend on their orientation relative to the cell strain. Interestingly, our model predicts that the ratio of bound actin filaments with different orientations ϕ_1, ϕ_2 increases exponentially with their strain difference

$$\frac{(\eta b)\,(\phi_2)}{(\eta b)\,(\phi_1)} = e^{\frac{\Delta\tilde{\mu}}{k_{\mathrm{B}}T}[\epsilon(\phi_2)-\epsilon(\phi_1)]}. \tag{7}$$

This implies that a static anisotropic strain leads to an alignment of the filaments in the direction of the maximal extensile strain as illustrated in figure 3b. These strain-dependencies

bioRxiv preprint doi: https://doi.org/10.64898/2026.11.09.762803; this version posted November 10, 2026. The copyright holder for this preprint (which was not certified by peer review) is the author/funder, who has granted bioRxiv a license to display the preprint in perpetuity. It is made available under a CC-BY 4.0 International license.

can be qualitatively understood as follows: If the cell contracts ($\epsilon < 0$) the actin filaments become compressed. As they remodel towards their relaxed state following equation (5) they lose actin monomers and thus also the number of cross links decreases. As a result, the total binding energy of the actin filament to the network decreases which finally leads to a higher dissociation rate and a lower concentration of bound actin in the steady state. We mention already here that a contraction of the cell can be caused by acto-myosin contraction which again depends on the actin network. This feedback will become crucial later to understand the formation of the actin structures in section III A.

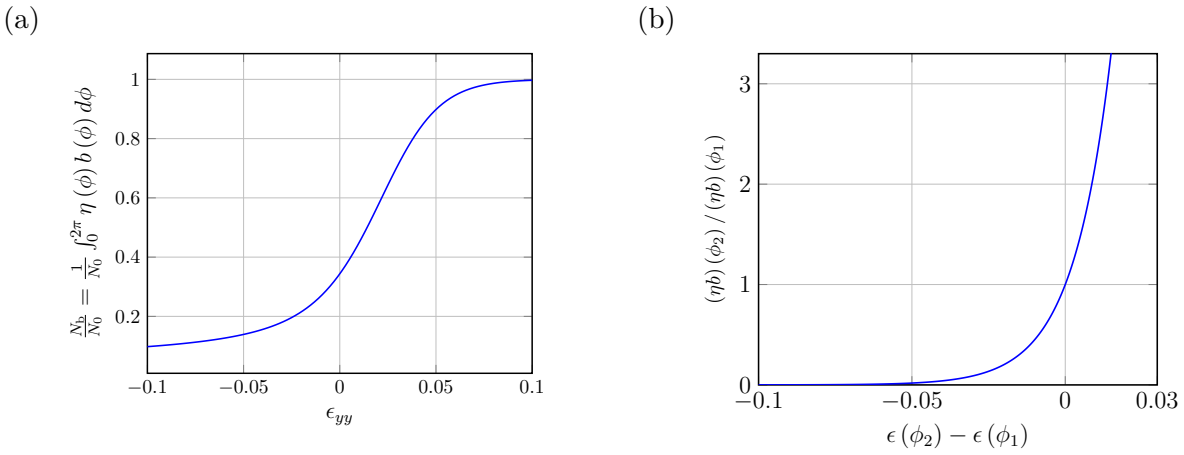


FIG. 3: Concentration and stress generation of the actin network in the steady state. (a) shows the dependency of the total concentration of bound monomers N_b on a uniaxial cell strain ϵ_{yy}. (b) shows the exponential dependency of the ratio of bound actin monomers in different orientations on the difference of the respective strains.

4. Active stress generation

To complete the model we now specify the active stress generated by the acto-myosin network. Active stresses arise when myosin complexes bind to two neighboring actin filaments, undergo a conformational change and then pull the actin filaments together [28]. As a result, the tension T depends on the actin network and thus the fields $\eta(\vec{x}, \phi), b(\vec{x}, \phi)$ and can be derived as follows. In our continuum model, all quantities including T are averages over a volume element which here is assumed to be small enough that maximally one myosin inside the volume is in its force generating state at a certain time. Then, the average tension

bioRxiv preprint doi: https://doi.org/10.64898/2026.11.09.762803; this version posted November 10, 2026. The copyright holder for this preprint (which was not certified by peer review) is the author/funder, who has granted bioRxiv a license to display the preprint in perpetuity. It is made available under a CC-BY 4.0 International license.

scales linearly with the time fraction in which one myosin complex is in its force generating state. This fraction, in turn, depends linearly on the total number of myosin binding sites which scales linearly with the number of actin monomers bound in the network. In total, the tension generated by filaments with orientation $\vec{n} = (\cos\phi, \sin\phi)$ scales as $T \sim \eta(\phi) \cdot b(\phi)$. Denoting as $T_{\max}$ the tension which is achieved when all actin polymerizes the tension per actin monomer is $\frac{T_{\max}}{N_0}$ and thus

$$T(\phi) = \frac{T_{\max}}{N_0}\eta(\phi)b(\phi). \tag{8}$$

From this, the full three-dimensional stress tensor σ_{ij} is obtained by integrating T over all directions ϕ and adding the passive stress $\sigma_{ij}^{(\text{pass})}$ from equation (2):

$$\begin{aligned}\sigma_{ij} &= \sigma_{ij}^{(\text{pass})} + \sigma_{ij}^{(\text{act})} \\ &= \sigma_{ij}^{(\text{pass})} + \int_0^{2\pi} n_i n_j T(\phi) d\phi \\ &= \sigma_{ij}^{(\text{pass})} + \frac{T_{\max}}{N_0}\int_0^{2\pi} n_i n_j \eta(\phi) b(\phi) d\phi.\end{aligned} \tag{9}$$

This stress tensor combined with the condition for a quasistatic force equilibrium

$$\partial_j \sigma_{ij} = 0, \tag{10}$$

together with the time evolution equations for the actin network (equations (3), (4) and (5)) fully specify our model in the cytoskeleton region outside the nucleus.

5. *Model for the nucleus*

Experimental data suggests that the nucleus behaves as a purely elastic material under physiological strains [36, 37]. Its elastic modulus is, however, not reliably known and is most likely not constant, since nuclear deformation might affect the cross linking of lamin proteins and chromatin organization increasing nuclear stiffness [38, 39]. As we are primarily interested in the influence of the actoymosin network on the nucleus we choose its elastic properties to be the same as the passive elastic properties of the rest of the cell. This implies that the deformation and normal stresses are continuous at the outer boundary of the nucleus. We found that the effects which we observe in this work do not change qualitatively when varying the nucleus' elastic modulus.

bioRxiv preprint doi: https://doi.org/10.64898/2026.11.09.762803; this version posted November 10, 2026. The copyright holder for this preprint (which was not certified by peer review) is the author/funder, who has granted bioRxiv a license to display the preprint in perpetuity. It is made available under a CC-BY 4.0 International license.

	active and passive stresses	
$T_{\max}$	maximum acto-myosin tension	$4kPa$
E	passive elastic modulus	$500Pa$
ν	Poisson ratio	0.45
	actin network dynamics	
$\Delta\tilde{\mu}$	dimensionless chemical potential difference of the unbound and bound state per monomer	$80k_BT$
ω_1	normalized binding rate	$0.05s^{-1}$
$\omega_2 e^{-\frac{\Delta\tilde{\mu}}{k_BT}}$	unbinding rate	$0.61s^{-1}$
τ	relaxation time of the actin filament remodeling process	$3.3s$

TABLE I: This table lists all the parameters of the model including the chosen values. A detailed justification for these choices is given in the text.

B. Parameter choice

In this section, the choice for the parameters employed in the following simulations will be presented and justified. To start, we note that the governing equations ((3), (4) and (5)) only depend on the ratios $b/b_0, \eta/\frac{N_0}{b_0}$ and N_u/N_0. Thus, the quantities N_0, b_0 can be eliminated by normalizing N_u, b, η accordingly and consequently do not need to be specified (see appendix A for the resulting equations). Furthermore, they do not explicitly depend on the cell size but only on the ratio $R_{\text{nucleus}}/R_{\text{cell}}$ which is set to 0.4. The values of all remaining parameters are listed in table I and will now be justified.

As passive elastic parameters we choose $E = 500Pa, \nu = 0.45$. The measured elastic response of cells varies heavily depending on the cell type, substrate and measurement method, but typical values lie around $E = 1kPa$ [40]. These measurements, however, represent overall values that do not separate the passive elastic response from the contribution of the acto-myosin network as we do in our model. To estimate only the former, we consider experiments [41, 42] which showed that the inhibition of the acto-myosin contractility significantly reduces the elastic modulus to around $30 - 50\%$ of its initial value. We therefore

bioRxiv preprint doi: https://doi.org/10.64898/2026.11.09.762803; this version posted November 10, 2026. The copyright holder for this preprint (which was not certified by peer review) is the author/funder, who has granted bioRxiv a license to display the preprint in perpetuity. It is made available under a CC-BY 4.0 International license.

use a smaller elastic modulus of $E = 500Pa$ for the passive contribution in our model. Next, we set the maximum contractile tension $T_{\max} = 4kPa$. This is based on measurements of the contractile tensions occurring in focal adhesions [43] which we expect to be close to the maximally achievable acto-myosin tensions in non-muscle cells.

For the dynamics of the actin network, in general, no direct experimental values are known such that only rough estimations can be made here. The difference of the chemical potential of the free and bound state $\Delta\tilde{\mu}$ determines the strain sensitivity of the actin network and thus the extent of the actin ring. We estimate $\Delta\tilde{\mu} = 80k_BT$ based on the binding energy of the cross links between two actin filaments. From molecular dynamics simulations binding energies per cross-linking molecule of around $10k_BT$ are reported [44–46]. The mesh size in cortical actin which lies around $20nm$ delivers a rough approximation for the distance between individual cross-linking sites. Individual actin filaments are $\sim 200nm$ long [47] and thus contain ~ 10 cross links which implies a total binding energy per actin filament in the order of magnitude $\Delta\tilde{\mu} \sim 100k_BT$. As the maximal strains occurring are ~ 0.1, the binding energy between an unstrained and a maximally strained filament differs maximally by $10k_BT$.

Next, the binding (polymerization) and unbinding (depolymerization) rates per filament are set as $\omega_1 = 0.05s^{-1}$ and $\omega_2 e^{-\frac{\Delta\tilde{\mu}}{k_B T}} = 0.61s^{-1}$. Assuming that the growth of the actin network by the incorporation of new actin monomers is the slowest time scale, the depolymerization rate $\omega_2 e^{-\frac{\Delta\tilde{\mu}}{k_B T}} = 0.61s^{-1}$ was fitted such that the model reproduced the experimental time scale for the occurrence of the perinuclear actin ring which is around $40s$ [13]. Subsequently, the polymerization rate ω_1 was fitted such that the extent of the actin ring becomes maximal.

Finally, the timescale for the remodeling of the actin network is set to $\tau = 3.3s$. This choice is motivated by the turnover timescales of the actin network which are known to be strongly influenced by the presence of several actin-binding proteins and vary from seconds in cortical actin and the lamellipodium up to hours for permanent structures like sarcomeres [48, 49]. As the actin structures considered here are rather disorganized we expect that their turnover times are similar to those in dynamic structures like the actin cortex and the lamellopodium, justifying the choice $\tau = 3.3s$. As a result, the remodeling is the significantly faster process. I.e. the incorporation of new filaments (ω_1, ω_2) is the limiting factor determining the timescale of the build-up of the actin ring, whereas the time scale of

bioRxiv preprint doi: https://doi.org/10.64898/2026.11.09.762803; this version posted November 10, 2026. The copyright holder for this preprint (which was not certified by peer review) is the author/funder, who has granted bioRxiv a license to display the preprint in perpetuity. It is made available under a CC-BY 4.0 International license.

the remodeling (τ) only weakly influences how fast the actin ring develops.

C. Numerical method

As we consider a two-dimensional domain, we discretized the cell (including the nucleus) using triangular linear elements. Typical resolutions for most of the simulations were $N_{\text{triangles}} = 10000$. The governing equations were solved using a homemade finite-element code. Directly around the nucleus a higher resolution was used ($\sim 4\times$ as high) to accurately resolve the actin ring. The displacement $\vec{u}$ was interpolated linearly over these elements while the fields η and b are considered constant within each triangle. Besides the spatial discretization, we discretized the orientational dependency of η and b using $N_\phi = 200$ points.

The orientational integrals were evaluated using the trapezoidal rule

$$\int_0^{2\pi} f(\phi)\, d\phi \to \frac{2\pi}{N_\phi} \sum_{j=0}^{N_\phi} f\left(\frac{j\pi}{N_\phi}\right) \tag{11}$$

where additionally the symmetry $\phi \leftrightarrow \phi + \pi$ was exploited.

For time stepping, the following scheme was used: Based on the current displacement and the resulting strain, for each triangle, the evolution equations for the actin network, (3) and (5), define a set of $2N_\phi$ ordinary differential equations which are independent for each triangle. Thus for each triangle the corresponding set of evolution equations was integrated using the Cash-Karp method. The stress tensor depends on the strain which can be expressed using the new displacements $\vec{u}(t + \Delta t)$ and the strain-rate which is also expressed in terms of the new displacements $\vec{u}(t + \Delta t)$ using forward differences: $\dot{\epsilon}_{ij} = \frac{\epsilon_{ij}(t+\Delta t) - \epsilon_{ij}(t)}{\Delta t}$. Using the condition for mechanic equilibrium $\partial_j \sigma_{ij} = 0$ we determined the new displacements $\vec{u}(t + \Delta t)$. During this step the new values for the actin fields η and b were used and $\dot{b}$ was determined using equation (5) by inserting the strain from the last time step. The nucleus was realized by not integrating the evolution equations for the triangles which make up the nucleus, implying $\eta = 0$ for all triangles whose initial centroid position is within R_{nucleus} from the nucleus center.

As initial conditions, we chose $\eta = 0, \frac{b}{b_0} = 1, \vec{u} = 0$.

bioRxiv preprint doi: https://doi.org/10.64898/2026.11.09.762803; this version posted November 10, 2026. The copyright holder for this preprint (which was not certified by peer review) is the author/funder, who has granted bioRxiv a license to display the preprint in perpetuity. It is made available under a CC-BY 4.0 International license.

III. RESULTS

Using the model presented above, we aim to understand two key experimental findings. We start with the formation of the perinuclear actin ring which is considered in the subsection III A. References [13] and [18] observed its formation upon a sudden mechanical stimulation which triggered an influx of calcium ions leading to a relatively homogeneous and instantaneous increase in the concentration of Ca^{2+}-ions. These activate the actin nucleator inverted formin 2. Intriguingly, although both the nucleator and the elevated concentration of Ca^{2+}-ions were present throughout the entire cell, only a highly localized actin ring around the nucleus formed. As we will show below, our model can explain this finding by the exponential dependence of actin depolymerization postulated in equation (3).

Next, we study the influence of the actin network on the positioning of the nucleus. In general, there exist a big variety of different mechanisms involved in the nucleus positioning which, next to acto-myosin contractility also include pushing forces exerted by actin polymerization or the activity of microtubule-associated motors [12]. Here, we restrict ourselves to model one particular situation: [19] studied the recentering of nuclei after their displacement by centrifugation and found that in certain situations it necessitates the binding of actin to the nucleus and acto-myosin contractility.

A. Formation of the perinuclear actin ring

We model the experiments of Shao et al. [13] starting from the moment directly after mechanical stimulation, when calcium is present throughout the cell, but actin polymerization has not yet started. Accordingly, we use the initial condition $\eta = 0$ and set $\omega_1 > 0$ as explained in subsection II B. When solving our model, we reach a steady state after $\approx 40s$. As shown in figure 4, we clearly find the formation of a perinuclear actin ring in agreement with the experimental observation. The spatial distribution of bound actin, $N_\mathrm{b}(\vec{x}) = \int_0^{2\pi} \eta\, b\, d\phi$, is shown in figure 4a demonstrating the ring as a thin region around the nucleus with an elevated actin concentration $N_\mathrm{b}/N_0 \approx 0.42$. At the outer edge of the cell a concentration of $N_\mathrm{b}/N_0 \approx 0.3$ is observed. Comparing with the unstressed reference concentration $N_\mathrm{b}^\mathrm{ref} = 0.34$ from section II A 3 c, we find that the presence of the nucleus induces actin polymerization near the nucleus and actin depolymerization in the cortex region.

bioRxiv preprint doi: https://doi.org/10.64898/2026.11.09.762803; this version posted November 10, 2026. The copyright holder for this preprint (which was not certified by peer review) is the author/funder, who has granted bioRxiv a license to display the preprint in perpetuity. It is made available under a CC-BY 4.0 International license.

Interestingly, depolymerization of cortical actin after a mechanical stimulus has also been observed experimentally by [13, 18]. Figure 4b shows the orientation of the actin filaments. The orientation distributions $(\eta b)(\phi)$ at different points are illustrated as polar plots. We observe that in addition to the higher concentration, the filaments in the actin ring are strongly aligned tangentially around the nucleus.

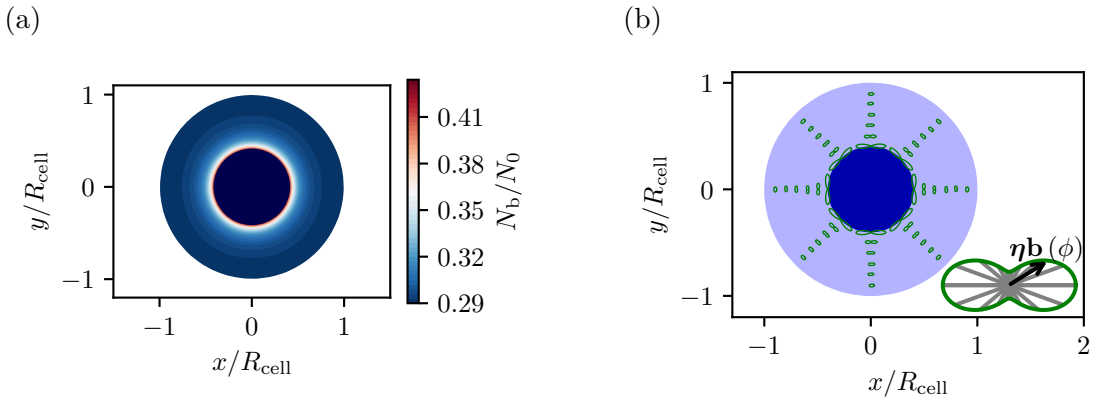


FIG. 4: Formation of the actin ring around the nucleus after mechanical stimulation. (a) shows the concentration of bound actin monomers throughout the cell. (b) shows the orientations of the actin filaments using polar plots of $\eta(\phi) \cdot b(\phi)$. The length of the arrow, i.e. the distance of the green curve from the center, indicates the local concentration of filaments with the respective orientation. Both plots show the situation when the steady state is reached.

To understand both the increased actin concentration near the nucleus as well as the tangential orientation of the perinuclear filaments, we consider the steady-state anisotropic cell strain shown in figure 5a. We first note that the acto-myosin contraction in the cytoskeleton leads to an isotropic expansion of the nucleus, i.e. $\epsilon_{\text{rr}} = \epsilon_{\phi\phi} > 0$ for $r/R_{\text{cell}} < 0.4$. This is consistent with the experimentally observed expansion during the mitotic exit triggered by actin polymerization [50] as well as its shrinking after the inhibition of myosin contraction or the depolymerization of actin [51]. Next, we consider the radial strain ϵ_{rr} outside the nucleus for $r/R_{\text{cell}} > 0.4$. Since the cell adheres to the substrate at its periphery the deformation $u = 0$ at $r/R = 1$. Accordingly, the expansion of the nucleus cannot be compensated by a corresponding expansion of the cytoskeleton and therefore the latter has to undergo radial contraction which leads to $\epsilon_{\text{rr}} < 0$ as shown in figure 5a. At the same time, the elongation of the nucleus perimeter causes a positive tangential strain $\epsilon_{\phi\phi}$ of the cytoskeleton around the

bioRxiv preprint doi: https://doi.org/10.64898/2026.11.09.762803; this version posted November 10, 2026. The copyright holder for this preprint (which was not certified by peer review) is the author/funder, who has granted bioRxiv a license to display the preprint in perpetuity. It is made available under a CC-BY 4.0 International license.

nucleus which vanishes towards the cell boundary as a result of the adhesive boundary condition $\vec{u} = 0$. Refering back to figure 3b, this leads to an increased depolymerization rate of radially oriented filaments and a decreased depolymerization rate of tangentially oriented filaments. This finally leads to the predominantly tangential alignment of the actin filaments. Refering back to the exponential dependence of the equilibrium actin concentration on cell strain (figure 3a) we see furthermore that the concentration increase of tangential filaments outweights the concentration decrease of radial filaments thus explaining the net increase of polymerized actin in the vicinity of the nucleus as shown in figure 4a. We conclude that the exponential strain dependence of the actin depolymerization rate postulated in equation (3) can be considered as the root cause for the formation of the perinuclear actin ring.

In our proposed mechanism, contractile actomyosin tensions play a central role for the formation of the actin ring. We therefore checked the sensitivity of the mechanism to the magnitude of the contractile stress by varying $T_{\max}$. In appendix B we show that even for an eight times smaller value of $T_{\max}$ our model still predicts formation of the actin ring. This is in agreement with the experiments in [13, 18] who found that the actin ring still occurred after adding blebbistatin which inhibits actomyosin contractile activity.

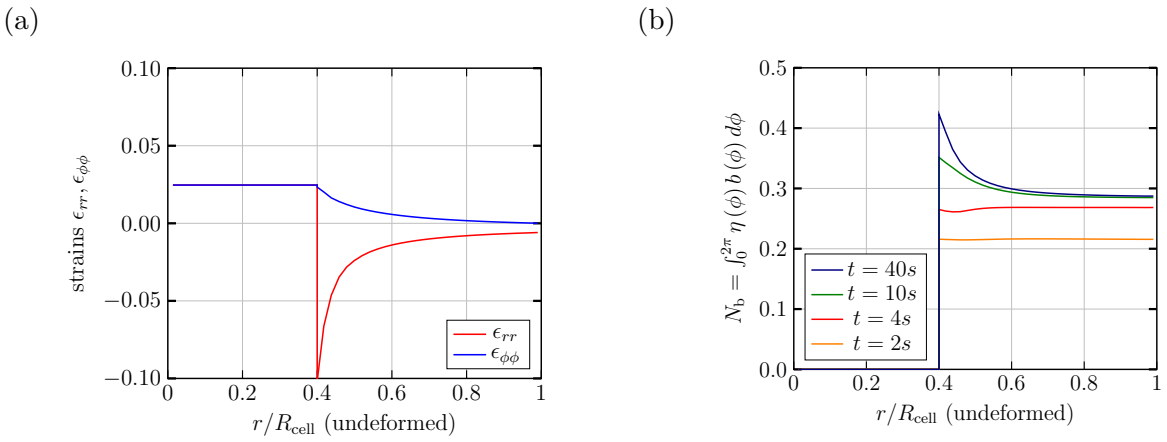


FIG. 5: (a) shows the cell strain split into radial and tangential components for the same situation as in figure 4. (b) illustrates the time evolution of the actin ring by showing the radial profiles of the total concentration of bound actin at different times.

Finally, we investigate the temporal dynamics of actin ring formation in figure 5b which shows the radial actin concentration profiles at different times. We predict that there is an initial transient of about $5s$ in which the actin concentration near the nucleus is actually

bioRxiv preprint doi: https://doi.org/10.64898/2026.11.09.762803; this version posted November 10, 2026. The copyright holder for this preprint (which was not certified by peer review) is the author/funder, who has granted bioRxiv a license to display the preprint in perpetuity. It is made available under a CC-BY 4.0 International license.

lower than in the periphery. However, this transient vanishes quickly and after about $40s$ the steady state as described in the previous paragraph is reached.

B. Recentering of the nucleus

Next to controlling its shape the actin cytoskeleton is also known to play a role in positioning the nucleus, e.g. during cell migration or nucleokinesis [9]. As a second application, we use our model to gain insight into the re-centering of an initially displaced nucleus as in the experiments of Zhu et al [19]. In these experiments, the nucleus was first moved to an off-centered position by centrifuging the cells, after which it was observed how the nucleus returned to its original position $\sim 20min$ after the centrifugation was stopped. To mimic this situation we use a passive elastic reference shape in which the nucleus is displaced from the center by $\delta y = 0.5R_{\text{cell}}$ and leave all other boundary conditions unchanged as in section III A. The resulting distribution of bound actin and its orientation are shown in figure 6.

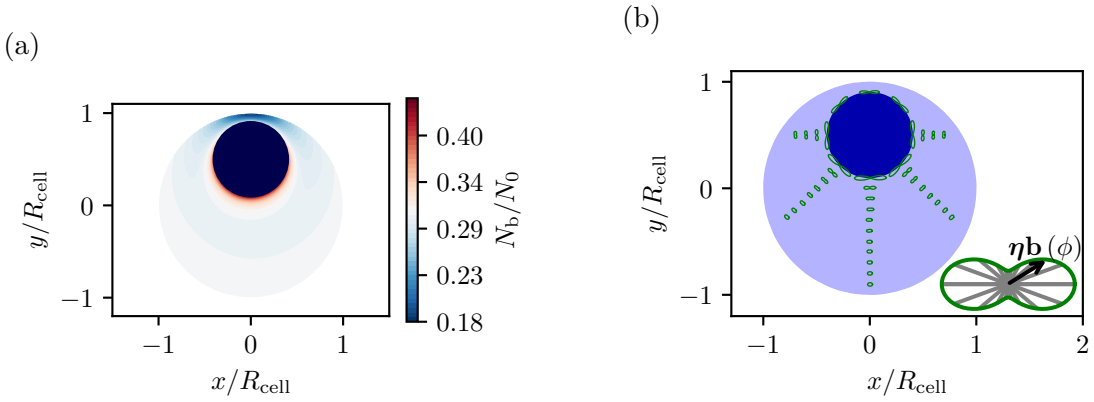


FIG. 6: Steady-state actin network in a cell with a displaced nucleus. (a) shows the corresponding total concentration of bound actin which is higher on the side of the nucleus facing the cell center. (b) shows the orientation distribution of the actin filaments in the steady state for a cell with a displaced nucleus.

Similar to the previous cases, the actin filaments are mainly oriented tangentially. In contrast to the previous situations, however, the actin concentration on the nucleus side facing the cell center is higher than on the side facing the boundary. The reason for this difference, according to our model, is that the strain on the side closer to the cell boundary

bioRxiv preprint doi: https://doi.org/10.64898/2026.11.09.762803; this version posted November 10, 2026. The copyright holder for this preprint (which was not certified by peer review) is the author/funder, who has granted bioRxiv a license to display the preprint in perpetuity. It is made available under a CC-BY 4.0 International license.

is lower due to the fixed cell edge. This lower strain leads to shorter filaments and thus to a higher depolymerization rate which reduces the concentration of actin filaments compared to the side facing the cell center. This discrepancy in concentrations leads to a discrepancy in acto-myosin induced stressess and, finally, to a force pulling the nucleus back to the cell center.

To obtain a quantitative estimate, we first calculate the force which is exerted by the acto-myosin contraction on the nucleus, by only considering the active part of the stress tensor from equation (9):

$$f_i = \int_{\partial(\text{nucleus})} \sigma_{ij}^{(\text{act})} n_j ds \tag{12}$$

Note that as we are always only considering a two-dimensional slice of the cell f_i is a force per unit height of the cell. We use a deflection of the nucleus $\delta y = 0.05 R_{\text{cell}}$, set the cell radius $R_{\text{cell}} = 30\mu m$ and choose a nucleus size of $R_{\text{nucleus}} = 0.4 R_{\text{cell}}$ as in the paragraphs above. For this situation, our model predicts a total force per height on the nucleus of $f_y \approx 6\frac{pN}{\mu m}$ as obtained by numerically evaluating the integral in equation (12) from our simulation results. As height of the cell, we use $h = 6\mu m$ which is a typical value for monolayers of the same fibroblast cell line [52] as used by Zhu et al [19] to study this recentering. To estimate the resulting velocity we assume that for very slow movements this force is compensated by the viscous drag which is very roughly $\sim 6\pi R_{\text{nucleus}} \eta v_{\text{recenter}}$. As typical value for the static viscosity of the cytoplasm we use $\mu \approx 60 Pa \cdot s$ as it was found for the same cell line via magnetic rotational spectroscopy [53, 54]. [1] With this, we finally obtain

$$v_{\text{recenter}} \sim \frac{f_y h}{6\pi\eta R_{\text{nucleus}}} \approx 0.16 \frac{\mu m}{min} \tag{13}$$

This result is close to the experimentally found recentering velocity of $v_{\text{recenter}} \sim 0.1\frac{\mu m}{min}$ which we estimated based on figure 2d) of Ref. [19]. This final application provides further evidence for the general applicability of our model, even beyond our initial motivation to explain the formation of a static perinuclear actin ring.

[1] This technique measures the local cytoplasmic viscosity inside the cell using rotating wires with lengths $L \approx 4\mu m$ and comparably small rotation speeds $\omega \approx 0.01 - 1\frac{rad}{s}$. As this length scale is relatively close to the size of the nucleus we expect this viscosity to be a good approximation for the viscosity experienced by the nucleus.

bioRxiv preprint doi: https://doi.org/10.64898/2026.11.09.762803; this version posted November 10, 2026. The copyright holder for this preprint (which was not certified by peer review) is the author/funder, who has granted bioRxiv a license to display the preprint in perpetuity. It is made available under a CC-BY 4.0 International license.

IV. CONCLUSION

We presented a theoretical model which predicts the formation of perinuclear actin structures triggered by a mechanical stimulus to biological cells, in agreement with experimental observations. The perinuclear structures exhibit an enhanced concentration of polymerized actin filaments together with a predominantly tangential filament orientation in a thin region around the nucleus. Importantly, our model does not require an enhanced concentration of nucleators or signaling molecules in the perinuclear region. Instead, the key mechanism in our model is an exponential decrease of the depolymerization rate as a function of the local mechanical strain. Together with active stress generation by myosin molecular motors bound to actin filaments, this creates a positive feedback loop leading to both enhanced concentration and tangential orientation of actin filaments in the perinuclear region. All ingredients of the model are microscopically motivated without ad-hoc assumptions and realistic, experimentally motivated values are used for all model parameters.

As a second application, we consider a cell whose nucleus is displaced from the cell center. In this situation, without any further ad-hoc assumptions, our model predicts the existence of a net force pushing the nucleus back towards the cell center. From this force, we can estimate the centripetal velocity with which the nucleus is expected to move which we find in quantitative agreement with experimental observations.

In conclusion, our model provides a generic, physics-based mechanism for the formation of localized actin structures without the need of specific spatial distributions of biochemical signaling molecules.

Appendix A: Non-dimensional governing equations

Here the non-dimensionalized equations for the evolution of the actin fields and the stress tensor are given. The actin fields are normalized via $b' = \frac{b}{b_0}, \eta' = \frac{b_0}{N_0}\eta, N'_{\mathrm{u}} = \frac{N_{\mathrm{u}}}{N_0}$. This way, the governing equations do not depend on the quantities N_0 and b_0 anymore:

bioRxiv preprint doi: https://doi.org/10.64898/2026.11.09.762803; this version posted November 10, 2026. The copyright holder for this preprint (which was not certified by peer review) is the author/funder, who has granted bioRxiv a license to display the preprint in perpetuity. It is made available under a CC-BY 4.0 International license.

$$\dot{b'} = -\frac{b' - (1+\epsilon)}{\tau} \begin{cases} 1 & \dot{b'} < 0 \\ N'_{\mathrm{u}} & \dot{b'} > 0 \end{cases} \tag{A1}$$

$$\dot{\eta'} = \omega_1 \frac{N'_{\mathrm{u}}}{b'} - \omega_2 \eta' e^{-b' \frac{\Delta\tilde{\mu}}{k_B T}} \tag{A2}$$

$$1 = N'_{\mathrm{u}} + \int_0^{2\pi} \eta'(\phi)\, b'(\phi)\, d\phi \tag{A3}$$

$$\sigma_{ij} = \frac{E\nu}{1-\nu^2}\epsilon_{kk}\delta_{ij} + \frac{E}{1+\nu}\epsilon_{ij} + T_{\max} \int_0^{2\pi} n_i n_j \eta'(\phi)\, b'(\phi)\, d\phi \tag{A4}$$

In the last expression ϵ_{ij} and σ_{ij} already denote the two-dimensional strain and stress tensors.

Appendix B: Sensitivity of the Actin Ring to acto-myosin contractility

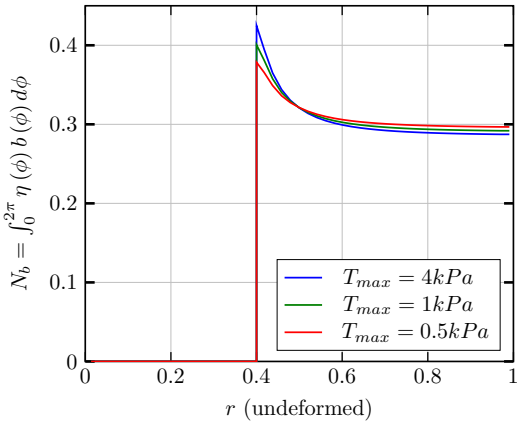


FIG. 7: To check the influence of the contractile tension $T_{\max}$ the radial profiles of bound actin achieved in the steady state (compare figure 5b) are plotted for different values of $T_{\max}$. It can be seen that even if the contractile tension is decreased by a factor of 8 a significant actin ring develops. This is consistent with the experimental observation that the actin ring also develops after the addition of blebbistatin which is known to decrease acto-myosin contractility, as discussed in the section III A.

bioRxiv preprint doi: https://doi.org/10.64898/2026.11.09.762803; this version posted November 10, 2026. The copyright holder for this preprint (which was not certified by peer review) is the author/funder, who has granted bioRxiv a license to display the preprint in perpetuity. It is made available under a CC-BY 4.0 International license.

ACKNOWLEDGMENTS

This work was funded by the Deutsche Forschungsgemeinschaft (DFG, German Research Foundation) under project number 546825574. B.B. acknowledges support from the Biological Physics study program of the Elite Network of Bavaria. This publication was funded by the University of Bayreuth Open Access Publishing Fund. Calculations were performed using the festus-cluster of the Bayreuth Centre for High Performance Computing funded by the Deutsche Forschungsgemeinschaft (DFG, German Research Foundation) under project number 523317330.

DATA AVAILABILITY

The simulation code and resulting data used to obtain the results of this work are available at Zenodo under DOI 10.5281/zenodo.22806150.

[1] G. Shivashankar, Mechanosignaling to the cell nucleus and gene regulation, Annual review of biophysics **40**, 361 (2011).

[2] E. Makhija, D. Jokhun, and G. Shivashankar, Nuclear deformability and telomere dynamics are regulated by cell geometric constraints, Proceedings of the National Academy of Sciences **113**, E32 (2016).

[3] T. Takaki, M. Montagner, M. P. Serres, M. Le Berre, M. Russell, L. Collinson, K. Szuhai, M. Howell, S. J. Boulton, E. Sahai, *et al.*, Actomyosin drives cancer cell nuclear dysmorphia and threatens genome stability, Nature communications **8**, 16013 (2017).

[4] X. Hu, Z. Z. Liu, X. Chen, V. P. Schulz, A. Kumar, A. A. Hartman, J. Weinstein, J. F. Johnston, E. C. Rodriguez, A. E. Eastman, *et al.*, Mkl1-actin pathway restricts chromatin accessibility and prevents mature pluripotency activation, Nature communications **10**, 1695 (2019).

[5] E. M. Hatch and M. W. Hetzer, Nuclear envelope rupture is induced by actin-based nucleus confinement, Journal of Cell Biology **215**, 27 (2016).

[6] T. Chancellor, J. Lee, C. K. Thodeti, and T. Lele, Actomyosin tension exerted on the nucleus through nesprin-1 connections influences endothelial cell adhesion, migration, and cyclic

bioRxiv preprint doi: https://doi.org/10.64898/2026.11.09.762803; this version posted November 10, 2026. The copyright holder for this preprint (which was not certified by peer review) is the author/funder, who has granted bioRxiv a license to display the preprint in perpetuity. It is made available under a CC-BY 4.0 International license.

strain-induced reorientation, Biophysical journal **99**, 115 (2010).

[7] J.-K. Kim, A. Louhghalam, G. Lee, B. W. Schafer, D. Wirtz, and D.-H. Kim, Nuclear lamin a/c harnesses the perinuclear apical actin cables to protect nuclear morphology, Nature communications **8**, 2123 (2017).

[8] H. T. Gilbert, V. Mallikarjun, O. Dobre, M. R. Jackson, R. Pedley, A. P. Gilmore, S. M. Richardson, and J. Swift, Nuclear decoupling is part of a rapid protein-level cellular response to high-intensity mechanical loading, Nature communications **10**, 4149 (2019).

[9] Y. Kalukula, A. D. Stephens, J. Lammerding, and S. Gabriele, Mechanics and functional consequences of nuclear deformations, Nature reviews Molecular cell biology **23**, 583 (2022).

[10] M. M. Nava, Y. A. Miroshnikova, L. C. Biggs, D. B. Whitefield, F. Metge, J. Boucas, H. Vihinen, E. Jokitalo, X. Li, J. M. G. Arcos, *et al.*, Heterochromatin-driven nuclear softening protects the genome against mechanical stress-induced damage, Cell **181**, 800 (2020).

[11] Z. Kechagia and P. Roca-Cusachs, Cytoskeletal safeguards: Protecting the nucleus from mechanical perturbations, Current Opinion in Biomedical Engineering **28**, 100494 (2023).

[12] P. M. Davidson, C. Denais, M. C. Bakshi, and J. Lammerding, Nuclear deformability constitutes a rate-limiting step during cell migration in 3-d environments, Cellular and molecular bioengineering **7**, 293 (2014).

[13] X. Shao, Q. Li, A. Mogilner, A. D. Bershadsky, and G. Shivashankar, Mechanical stimulation induces formin-dependent assembly of a perinuclear actin rim, Proceedings of the National Academy of Sciences **112**, E2595 (2015).

[14] S. B. Khatau, C. M. Hale, P. Stewart-Hutchinson, M. S. Patel, C. L. Stewart, P. C. Searson, D. Hodzic, and D. Wirtz, A perinuclear actin cap regulates nuclear shape, Proceedings of the National Academy of Sciences **106**, 19017 (2009).

[15] K. Nagayama and T. Fukuei, Cyclic stretch-induced mechanical stress to the cell nucleus inhibits ultraviolet radiation-induced dna damage, Biomechanics and modeling in mechanobiology **19**, 493 (2020).

[16] A. Zemel, Active mechanical coupling between the nucleus, cytoskeleton and the extracellular matrix, and the implications for perinuclear actomyosin organization, Soft matter **11**, 2353 (2015).

[17] Y. Zeng, A. K. Yip, S.-K. Teo, and K.-H. Chiam, A three-dimensional random network model of the cytoskeleton and its role in mechanotransduction and nucleus deformation, Biomechan-

bioRxiv preprint doi: https://doi.org/10.64898/2026.11.09.762803; this version posted November 10, 2026. The copyright holder for this preprint (which was not certified by peer review) is the author/funder, who has granted bioRxiv a license to display the preprint in perpetuity. It is made available under a CC-BY 4.0 International license.

ics and modeling in mechanobiology **11**, 49 (2012).

[18] P. Wales, C. E. Schuberth, R. Aufschnaiter, J. Fels, I. García-Aguilar, A. Janning, C. P. Dlugos, M. Schäfer-Herte, C. Klingner, M. Wälte, *et al.*, Calcium-mediated actin reset (caar) mediates acute cell adaptations, elife **5**, e19850 (2016).

[19] R. Zhu, S. Antoku, and G. G. Gundersen, Centrifugal displacement of nuclei reveals multiple linc complex mechanisms for homeostatic nuclear positioning, Current Biology **27**, 3097 (2017).

[20] J. Prost, F. Jülicher, and J.-F. Joanny, Active gel physics, Nature physics **11**, 111 (2015).

[21] A.-C. Reymann, F. Staniscia, A. Erzberger, G. Salbreux, and S. W. Grill, Cortical flow aligns actin filaments to form a furrow, Elife **5**, e17807 (2016).

[22] F. Jülicher, S. W. Grill, and G. Salbreux, Hydrodynamic theory of active matter, Reports on Progress in Physics **81**, 076601 (2018).

[23] V. S. Deshpande, R. M. McMeeking, and A. G. Evans, A bio-chemo-mechanical model for cell contractility, Proceedings of the National Academy of Sciences **103**, 14015 (2006).

[24] A. Vigliotti, W. Ronan, F. Baaijens, and V. Deshpande, A thermodynamically motivated model for stress-fiber reorganization, Biomechanics and modeling in mechanobiology **15**, 761 (2016).

[25] C. Obbink-Huizer, C. W. Oomens, S. Loerakker, J. Foolen, C. V. Bouten, and F. P. Baaijens, Computational model predicts cell orientation in response to a range of mechanical stimuli, Biomechanics and modeling in mechanobiology **13**, 227 (2014).

[26] F. J. Vernerey and M. Farsad, A constrained mixture approach to mechano-sensing and force generation in contractile cells, Journal of the mechanical behavior of biomedical materials **4**, 1683 (2011).

[27] W. Ronan, V. S. Deshpande, R. M. McMeeking, and J. P. McGarry, Cellular contractility and substrate elasticity: a numerical investigation of the actin cytoskeleton and cell adhesion, Biomechanics and modeling in mechanobiology **13**, 417 (2014).

[28] G. H. Koenderink and E. K. Paluch, Architecture shapes contractility in actomyosin networks, Current opinion in cell biology **50**, 79 (2018).

[29] G. Dimchev, B. Amiri, F. Fäßler, M. Falcke, and F. K. Schur, Computational toolbox for ultrastructural quantitative analysis of filament networks in cryo-et data, Journal of Structural Biology **213**, 107808 (2021).

bioRxiv preprint doi: https://doi.org/10.64898/2026.11.09.762803; this version posted November 10, 2026. The copyright holder for this preprint (which was not certified by peer review) is the author/funder, who has granted bioRxiv a license to display the preprint in perpetuity. It is made available under a CC-BY 4.0 International license.

[30] L. P. Cramer, M. Siebert, and T. J. Mitchison, Identification of novel graded polarity actin filament bundles in locomoting heart fibroblasts: implications for the generation of motile force, The Journal of cell biology **136**, 1287 (1997).

[31] T. Vignaud, C. Copos, C. Leterrier, M. Toro-Nahuelpan, Q. Tseng, J. Mahamid, L. Blanchoin, A. Mogilner, M. Théry, and L. Kurzawa, Stress fibres are embedded in a contractile cortical network, Nature materials **20**, 410 (2021).

[32] J. P. McGarry, J. Fu, M. T. Yang, C. S. Chen, R. M. McMeeking, A. G. Evans, and V. S. Deshpande, Simulation of the contractile response of cells on an array of micro-posts, Philosophical Transactions of the Royal Society A: Mathematical, Physical and Engineering Sciences **367**, 3477 (2009), https://royalsocietypublishing.org/rsta/article-pdf/367/1902/3477/1336058/rsta.2009.0097.pdf.

[33] A. B. Buskermolen, T. Ristori, D. Mostert, M. C. van Turnhout, S. S. Shishvan, S. Loerakker, N. A. Kurniawan, V. S. Deshpande, and C. V. Bouten, Cellular contact guidance emerges from gap avoidance, Cell Reports Physical Science **1** (2020).

[34] J. L. McGrath, Y. Tardy, C. Dewey, J. Meister, and J. Hartwig, Simultaneous measurements of actin filament turnover, filament fraction, and monomer diffusion in endothelial cells, Biophysical journal **75**, 2070 (1998).

[35] D. Zicha, I. M. Dobbie, M. R. Holt, J. Monypenny, D. Y. Soong, C. Gray, and G. A. Dunn, Rapid actin transport during cell protrusion, Science **300**, 142 (2003).

[36] T. P. Lele, R. B. Dickinson, and G. G. Gundersen, Mechanical principles of nuclear shaping and positioning, Journal of Cell Biology **217**, 3330 (2018).

[37] A. D. Stephens, E. J. Banigan, S. A. Adam, R. D. Goldman, and J. F. Marko, Chromatin and lamin a determine two different mechanical response regimes of the cell nucleus, Molecular biology of the cell **28**, 1984 (2017).

[38] S.-J. Heo, S. D. Thorpe, T. P. Driscoll, R. L. Duncan, D. A. Lee, and R. L. Mauck, Biophysical regulation of chromatin architecture instills a mechanical memory in mesenchymal stem cells, Scientific reports **5**, 16895 (2015).

[39] K. V. Iyer, S. Pulford, A. Mogilner, and G. Shivashankar, Mechanical activation of cells induces chromatin remodeling preceding mkl nuclear transport, Biophysical journal **103**, 1416 (2012).

[40] P.-H. Wu, D. R.-B. Aroush, A. Asnacios, W.-C. Chen, M. E. Dokukin, B. L. Doss, P. Durand-Smet, A. Ekpenyong, J. Guck, N. V. Guz, *et al.*, A comparison of methods to assess cell

bioRxiv preprint doi: https://doi.org/10.64898/2026.11.09.762803; this version posted November 10, 2026. The copyright holder for this preprint (which was not certified by peer review) is the author/funder, who has granted bioRxiv a license to display the preprint in perpetuity. It is made available under a CC-BY 4.0 International license.

mechanical properties, Nature methods **15**, 491 (2018).

[41] E. Moeendarbary, L. Valon, M. Fritzsche, A. R. Harris, D. A. Moulding, A. J. Thrasher, E. Stride, L. Mahadevan, and G. T. Charras, The cytoplasm of living cells behaves as a poroelastic material, Nature materials **12**, 253 (2013).

[42] J. C. Martens and M. Radmacher, Softening of the actin cytoskeleton by inhibition of myosin ii, Pflügers Archiv-European Journal of Physiology **456**, 95 (2008).

[43] N. Q. Balaban, U. S. Schwarz, D. Riveline, P. Goichberg, G. Tzur, I. Sabanay, D. Mahalu, S. Safran, A. Bershadsky, L. Addadi, *et al.*, Force and focal adhesion assembly: a close relationship studied using elastic micropatterned substrates, Nature cell biology **3**, 466 (2001).

[44] D. Sept and J. A. McCammon, Thermodynamics and kinetics of actin filament nucleation, Biophysical journal **81**, 667 (2001).

[45] L. Yang, D. Sept, and A. Carlsson, Energetics and dynamics of constrained actin filament bundling, Biophysical journal **90**, 4295 (2006).

[46] S. Zhang and D. Vavylonis, Steps of actin filament branch formation by arp2/3 complex investigated with coarse-grained molecular dynamics, Biophysical Journal **122**, 26a (2023).

[47] M. Kovács, J. Tóth, C. Hetényi, A. Málnási-Csizmadia, and J. R. Sellers, Mechanism of blebbistatin inhibition of myosin ii, Journal of Biological Chemistry **279**, 35557 (2004).

[48] M. Fritzsche, A. Lewalle, T. Duke, K. Kruse, and G. Charras, Analysis of turnover dynamics of the submembranous actin cortex, Molecular biology of the cell **24**, 757 (2013).

[49] B. L. Goode, J. Eskin, and S. Shekhar, Mechanisms of actin disassembly and turnover, Journal of Cell Biology **222**, e202309021 (2023).

[50] C. Baarlink, M. Plessner, A. Sherrard, K. Morita, S. Misu, D. Virant, E.-M. Kleinschnitz, R. Harniman, D. Alibhai, S. Baumeister, *et al.*, A transient pool of nuclear f-actin at mitotic exit controls chromatin organization, Nature cell biology **19**, 1389 (2017).

[51] A. Mazumder and G. V. Shivashankar, Emergence of a prestressed eukaryotic nucleus during cellular differentiation and development, Journal of The Royal Society Interface **7**, S321 (2010).

[52] Y. Liu, K. Mollaeian, and J. Ren, Finite element modeling of living cells for afm indentation-based biomechanical characterization, Micron **116**, 108 (2019).

[53] J.-F. Berret, Local viscoelasticity of living cells measured by rotational magnetic spectroscopy, Nature communications **7**, 10134 (2016).

bioRxiv preprint doi: https://doi.org/10.64898/2026.11.09.762803; this version posted November 10, 2026. The copyright holder for this preprint (which was not certified by peer review) is the author/funder, who has granted bioRxiv a license to display the preprint in perpetuity. It is made available under a CC-BY 4.0 International license.

[54] M. Dessard, J.-B. Manneville, and J.-F. Berret, Cytoplasmic viscosity is a potential biomarker for metastatic breast cancer cells, Nanoscale Advances **6**, 1727 (2024).